PHYSICAL REVIEW B **84**, 104525 (2011)

Experimental observation of thermal fluctuations in single superconducting Pb nanoparticles through tunneling measurements

Ivan Brihuega,[1,2] Antonio M. García-García,[3,4,*] Pedro Ribeiro,[4,†] Miguel M. Ugeda,[1,2] Christian H. Michaelis,[1] Sangita Bose,[1,5,‡] and Klaus Kern[1,6]

[1]*Max Planck Institute for Solid State Research, Heisenbergstrasse 1, Stuttgart, D-70569, Germany*

[2]*Departamento de Física de la Materia Condensada, Universidad Autónoma de Madrid, E-28049 Madrid, Spain*

[3]*T.C.M. Group, Cavendish Laboratory, University of Cambridge, J. J. Thomson Avenue, Cambridge CB3 0HE, United Kingdom*

[4]*CFIF, Instituto Superior Técnico, UTL, Av. Rovisco Pais, 1049-001 Lisboa, Portugal*

[5]*Center for Excellence in Basic Sciences, University of Mumbai, Vidhyanagari Campus, Mumbai-400098, India*

[6]*Institut de Physique de la Matière Condensée, Ecole Polytechnique Fédérale de Lausanne, CH-1015 Lausanne, Switzerland*

(Received 5 May 2011; revised manuscript received 5 July 2011; published 30 September 2011)

An important question in the physics of superconducting nanostructures is the role of thermal fluctuations (TFs) on superconductivity in the zero-dimensional limit. Here, we probe the evolution of superconductivity as a function of temperature and particle size in single, isolated Pb nanoparticles. Accurate determination of the size and shape of each nanoparticle makes our system a good model to quantitatively compare the experimental findings with theoretical predictions. In particular we study the role of TFs on the tunneling density of states (DOS) and the superconducting energy gap (Δ) in these nanoparticles. For the smallest particles $h \leqslant 13$ nm, we clearly observe a finite energy gap beyond T_c giving rise to a "critical region." We show explicitly through quantitative theoretical calculations that these deviations from mean-field predictions are caused by TFs. Moreover, for $T \ll T_c$, where TFs are negligible and typical sizes below 20 nm, we show that Δ gradually decreases with reduction in particle size. This result is described by a theoretical model that includes finite size effects and zero temperature leading order corrections to the mean-field formalism.

DOI: 10.1103/PhysRevB.84.104525 PACS number(s): 74.55.+v, 74.25.Bt, 74.78.Na

I. INTRODUCTION

Superconductivity in quantum confined systems has been a subject of research for the past few decades.[1–3] However, recent findings promoted by technological developments have revived the interest in this field.[4–18] These advances can shed light on the evolution of the ground state with particle size or the role of (thermodynamic) fluctuations on the stability of the superconducting state. Many earlier reports[19–23] have addressed some of these questions. However, a complete understanding of these problems is far from complete, though some general features are broadly accepted.

The effect of thermal fluctuations (TFs) on superconductivity in small particles has been probed previously in ensemble-averaged nanoparticle systems through studies of specific heat and diamagnetism.[24–26] It is known that as the dimension of the system is reduced below the superconducting coherence length (ξ), there are deviations from mean-field behavior due to quantum and TFs that lead to the smearing of the superconducting transition.[27] Interesting effects arise above the transition temperature (T_c) like the appearance of excess diamagnetism, conductivity, specific heat, and tunneling currents. A "critical regime" can thus be defined where superconducting fluctuations dominate. In a zero-dimensional superconductor where all dimensions are less than ξ, fluctuation effects lead to a large critical regime, which in principle can be accessed experimentally. A detailed study of this critical regime is possible only through measurements on single, isolated superconducting nanoparticles. Moreover, a good knowledge of the geometry of the system is required to carry out a quantitative comparison between experiments and theory.

In this paper we present an experimental study of the evolution of superconductivity in single, isolated nanoparticles as a function of size and temperature which overcomes these challenges. Through our scanning tunneling microscopy (STM) measurements on individual Pb nanoparticles with sizes ranging between 3–30 nm grown *in situ* in ultrahigh vacuum (UHV) conditions, we have addressed two fundamental questions: In the low temperature limit, how does superconductivity evolve as the particle size is decreased? For higher temperatures, how do TFs affect the tunneling DOS and hence superconductivity? In order to answer quantitatively these questions we have compared the experimental results to the theoretical predictions of a model that includes both TFs in the static path approximation (SPA),[28,29] finite-size corrections to mean field, and the leading corrections to the mean-field formalism at zero temperature.

The paper is structured as follows. After this introduction, in Sec. II sample preparation and the experimental methodology to obtain the superconducting energy gap (Δ) of the Pb nanoparticles are presented. In Sec. III A we provide a theoretical description of the DOS and the superconducting gap (Δ) based on the path integral formalism that describes the effect of TFs at $T \sim T_c$. Section III B theoretically addresses the low temperature regime ($T \ll T_c$) including deviations from mean-field predictions according to the Richardson formalism. The main results are presented and discussed in Sec. IV, where the evolution of Δ with the particle size in the low temperature limit and the TFs giving rise to a finite gap for $T > T_c$ are shown in IV A and IV B, respectively. In Sec. V the validity of the Dynes expressions in the nanoscale regime and the role of the broadening parameter $\Gamma(T)$ are investigated. Finally the main conclusions of the present work are summarized in Sec. VI.

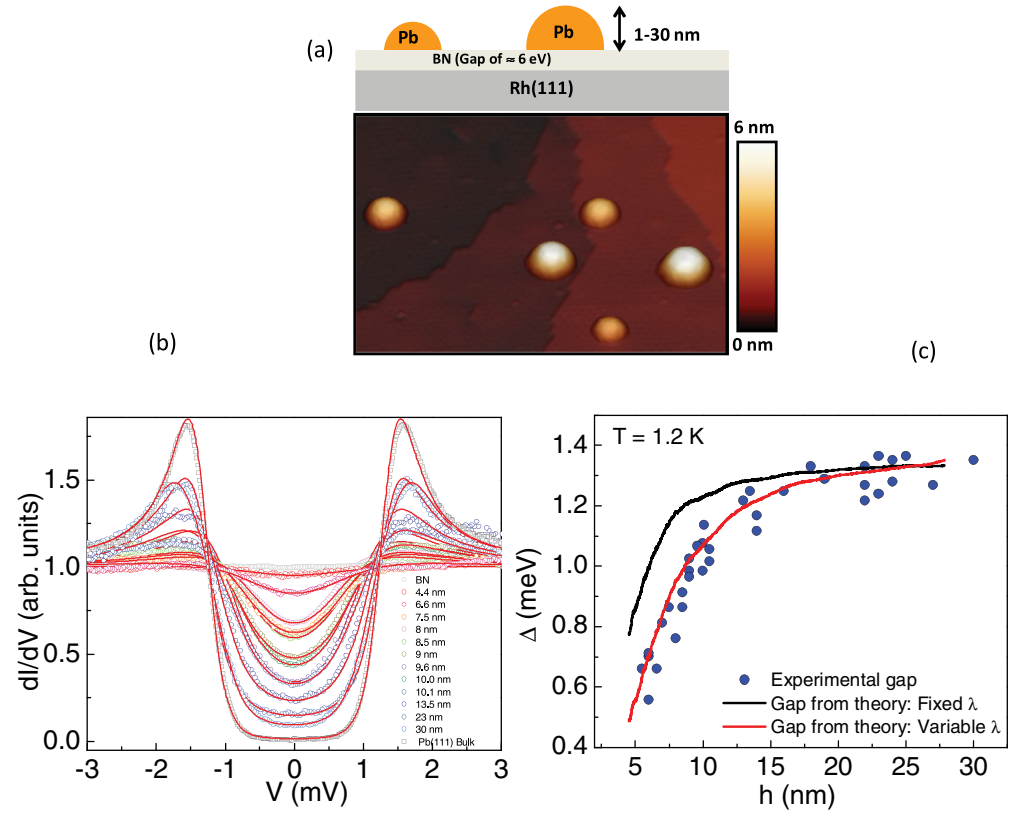

FIG. 1. (Color online) (a) The top panel shows a schematic of the isolated Pb nanoparticles on the BN/Rh(111) substrate. The lower panel is a typical STM image (162 × 125 nm^2) showing the general morphology of the isolated Pb nanoparticles of different sizes (3D plot obtained with the WSxM[40]) taken at a bias voltage of 1 V and a tunneling current of 0.1 nA. (b) Conductance spectra for particles with different sizes and $T = 1.1$–1.25 K. The symbols denote the experimental raw data. The solid lines are the best fitting using (1) with the DOS N_s given by the Dynes expression (2). Open squares correspond to a reference spectra measured in a Pb single crystal at 1.5 K. (c) Experimental (blue circles) and theoretical (solid lines) of the average superconducting energy gap for $T = 1.2$ K as a function of particle size (h). In the black theoretical curve it was assumed that the electron-phonon coupling $\lambda = 0.385$ does not depend on the particle size. In the red theoretical curve a size dependent $\lambda(h)$ is taken (see Appendix (4) and Fig. 8).

II. EXPERIMENTAL METHODS

The experiments were performed in a UHV system (base pressure $<5\times10^{-11}$ Torr) combined with a home-built ^{3}He low-temperature STM. Pb-isolated nanoparticles of 3–30-nm height were grown *in situ* on top of a BN/Rh(111) surface by means of buffer layer assisted growth (BLAG) [see Fig. 1(a)]. BN, an ultrathin insulating layer with an electronic gap of 5–6 eV and a thickness of ~0.25 nm, electronically decouples the particles from the metallic Rh(111) substrate[30] (for details of the preparation see Appendix (1)). Our high resolution STM images reveal that particles are hemispherical to a good approximation (see Appendix (1)). Differential conductance spectra (dI/dV vs V) were measured with a tungsten (W) tip on each nanoparticle with different heights using the lock-in technique (50 μV at 830 Hz voltage modulation). A stabilization current of 0.1 nA and an initial sample voltage of 8.0 mV was used to measure all the tunneling spectra. The additional energy broadening (other than thermal broadening) due to instrumental noise in our system was calibrated by measuring the tunneling conductance of a Pb(111) single crystal at 1.5 K [open squares in Fig. 1(b)]. An upper limit to the contribution of the broadening of the spectra due to an additional instrumental noise of 20 μeV at 1.5 K was obtained (see (Appendix (2)) for details). The calibration of the sample temperature was performed by measuring the superconducting critical temperature for bulk Pb, and the expected T_c of 7.25 K was obtained (see Appendix (2)).

Figure 1(b) shows unprocessed experimental dI/dV spectra measured at $T \ll T_c$ for different particle sizes, which gives their DOS. We fitted the curves with the tunneling equation[31]

$$G(V) = \left.\frac{dI}{dV}\right|_V = G_{nn}\frac{d}{dV} \times \left\{\int_{-\infty}^{\infty} N_s(E,\Delta,\Gamma)\{f(E) - f(E - \mathrm{eV})\}\,dE\right\}, \quad (1)$$

where $N_s(E, \Delta, \Gamma)$ is the DOS of the superconductor, $f(E)$ is the Fermi-Dirac distribution function, G_{nn} is the conductance of the tunnel junction for $V \gg \Delta/e$, and Γ is an effective broadening parameter, which in bulk superconductors is related to the quasiparticle lifetime.[32,33] As will be shown in Sec. V, in the case of nanoparticles it can also have contributions from TFs.

In Pb, a strong-coupled superconductor, $N_s(E, \Delta, \Gamma)$ should in principle be obtained directly from the Eliashberg's

mean-field formalism, which accounts for recombination processes and electron-phonon scattering. However a simpler DOS ansatz was proposed by Dynes and coworkers:[32]

$$N_s(E,\Delta,\Gamma) = \mathrm{Re}\left[\frac{|E| + i\Gamma(T)}{\sqrt{(|E| + i\Gamma(T))^2 - \Delta(T)^2}}\right]. \quad (2)$$

This is broadly used since the values of Δ and Γ thus obtained are in excellent agreement with the theoretical predictions of the Eliashberg's formalism. We used Eqs. (1) and (2) to fit our experimental spectra with Δ and Γ as fitting parameters. As can be seen in Fig. 1(b), there is an excellent agreement between the experimental data and the theoretical fits giving unique values of $\Delta(T)$ and $\Gamma(T)$, which characterizes ideally the superconducting state of each Pb nanoparticle (see (Appendix (2)) for the description of the fitting procedure).

Solid symbols in Fig. 1(c) show the size variation of the experimental superconducting gap Δ for low temperatures T = 1.1–1.25 K obtained from the fits using Eqs. (1) and (2). We observe that for large particles (>20 nm), Δ is similar to that of bulk Pb (∼1.36 meV) and subsequently decreases gradually as particle size is reduced.

III. THEORETICAL ASPECTS OF SUPERCONDUCTIVITY IN A ZERO-DIMENSIONAL SUPERCONDUCTOR

Although Dynes ansatz nicely reproduces the experimental conductance spectra (see Figs. 1 and 2), it does not give any information about the physical phenomena relevant at these length scales. One of the main goals of this paper is to overcome this limitation by providing a quantitative theoretical description of the experimental results. For that purpose we combine different theoretical tools from the path integral formalism in the SPA for T $\sim$ T_c to Richardson's equations that describe deviation from mean-field results in the low temperature limit. In the following we provide an introduction to these techniques.

A. T $\sim$ T_c: Description of TFs by the path integral formalism

The path integral formalism in the so-called SPA[28] is a powerful tool to describe the interplay between superconductivity and TFs in a zero-dimensional nanoparticle. We note that for $T \ll T_c$, corrections to mean field due to TFs are small, and other effects not included in SPA become relevant. Consequently other techniques, such as the Richardson formalism, must be employed in order to describe superconductivity beyond the mean-field limit in this region (see next section).

SPA assumes Δ to be space-time homogenous and can be used in our case as the system size is lower than the coherence length. Explicit analytical results are obtained for the DOS and Δ using this treatment, as described subsequently.

Superconductivity in the nanoparticle is modeled by the usual Bardeen-Cooper-Schrieffer (BCS) Hamiltonian,

$$H = \sum_{\alpha} \varepsilon_\alpha c_\alpha^\dagger - \lambda\delta \sum_{\alpha,\alpha'>0} c_\alpha^\dagger c_{-\alpha}^\dagger c_{-\alpha'} c_{-\alpha},$$

where λ is the coupling constant that describes the effective electron-phonon attraction, δ is the mean level spacing, ε_α are the eigenvalues of the one-body problem (for a free particle in almost hemispherical geometry). States labeled by α and $-\alpha$ are related by time-reversal symmetry. By a Hubbard-Stratonovich transformation, the partition function of the system ($Z = \mathrm{Tr}[e^{-\beta H}]$) can be expressed in terms of a complex gap variable $\Delta(\tau,r)$. The spatial dependence of $\Delta(\tau,r) \approx \Delta(\tau)$ is negligible since the coherence length of metallic particles is typically larger than the particle size. It is worth noting that the imaginary time dependence of

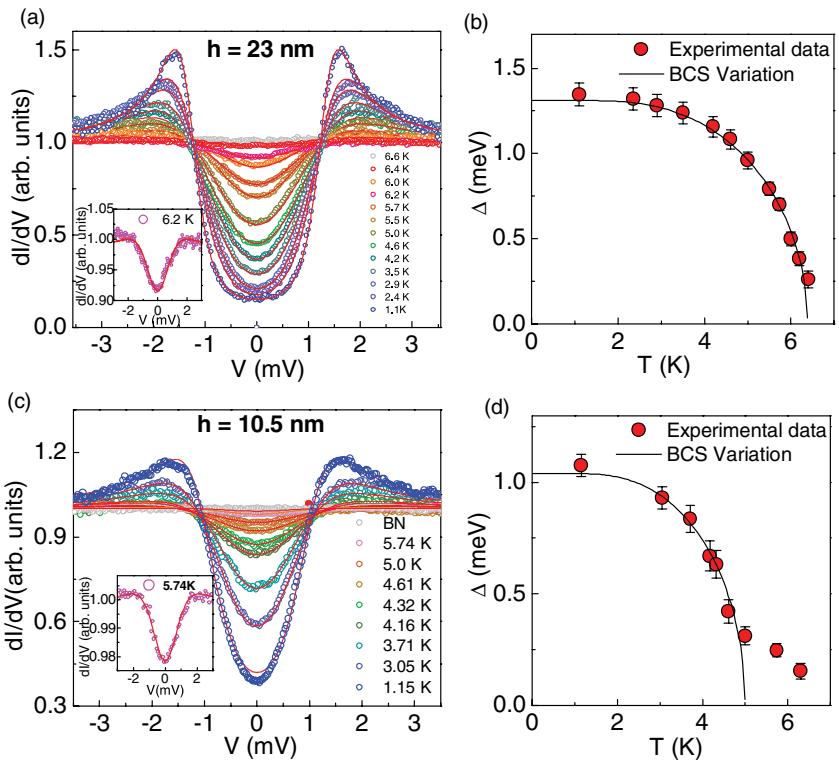

FIG. 2. (Color online) Conductance spectra vs temperature T for two particles of heights (a) 23 nm and (c) 10.5 nm. Experimental raw data are shown by open circles. Data in ash is taken at a temperature where no superconducting signal is obtained. The solid lines are the fits using Eqs. (1) and (2). For clarity the inset in Figs. 2(a) and 2(c) show the excellent fit to the conductance spectra at temperatures close to T_c where the signal changes by 2–8% from the background. (b), (d) show the variation of $\Delta(T)$ (red solid circles) with temperature (T) for the two particles as obtained from the fits. Solid lines correspond to the variation expected from BCS theory.

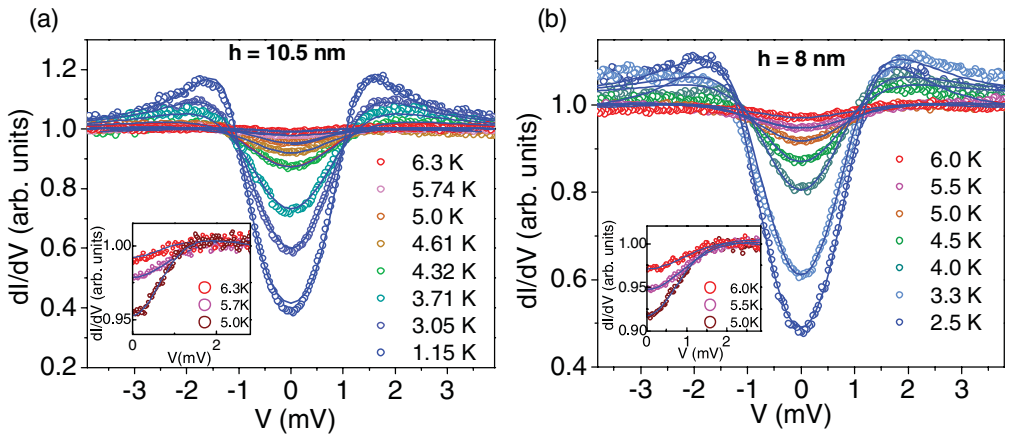

FIG. 3. (Color online) (a) Conductance spectra for particle with height $h = 10.5$ nm at different temperatures between $T = 1.0$–6.5 K. The symbols denote the experimental raw data. The solid lines are the best fits using Eq. (1) with the DOS N_s given by the SPA expression Eq. (3a). (b) The same for $h = 8$ nm. The insets in the two show a magnified scale where spectra close to and greater than T_c have been plotted. The clear signal above the background at these temperatures clearly demonstrates that the energy gap does not go to zero at T_c, and we see the effect of fluctuations on the tunneling DOS. For clarity we show the spectra only for positive voltage.

the energy gap is related to quantum fluctuations (QFs). We show in Sec. III B that for Pb this contribution is only relevant for particles with a typical size, $h < 5$ nm. Therefore to a good approximation the complex gap variable is also homogenous in time. This amounts to completely neglecting QFs but keeping TFs in the partition function [Eq. (3b)].We determine Z explicitly, which permits us to compute different observables related to the experimental results like the DOS and the superconducting energy gap (Δ).

1. DOS

The normalized DOS, $N_s(\omega)$, is related to the imaginary time Green's function $g(\omega + i\Gamma,\alpha)$ by $N_s(\omega) = -\lim_{\Gamma\to 0^+} \frac{1}{\pi N}\sum_\alpha \mathrm{Im}[g(\omega + i\Gamma,\alpha)]$. In the SPA approach Green's function is given by

$$g(i\omega_n,\alpha) = \left(\frac{z}{z_0}\right)^{-1}\int_0^\infty d\Delta\Delta e^{-\beta A(|\Delta|)} g_D(i\omega_n,\alpha),$$

where $g_D(i\omega_n,\alpha)$ is the usual superconducting Green's function. We simplify this expression to obtain the DOS given by

$$N_s(\omega) = \left(\frac{z}{z_0}\right)^{-1}\int_0^\infty d\Delta\Delta e^{-\beta A(|\Delta|)}\mathrm{Im}\left[\frac{\omega + \mathrm{i}\Gamma}{\sqrt{\Delta^2 - (\omega + \mathrm{i}\Gamma)^2}}\right] \quad (3a)$$

$$\frac{z}{z_0} = \int_0^\infty d\Delta\Delta e^{-\beta A(|\Delta|)}, \quad (3b)$$

with $A(|\Delta|) = \{(\lambda\delta)^{-1}|\Delta|^2 + \sum_\alpha(|\varepsilon_\alpha| - \xi_\alpha) - \frac{2}{\beta}\log(\frac{e^{-\beta\xi_\alpha}+1}{e^{-\beta|\varepsilon_\alpha|}+1})\}$; $\xi_\alpha = \sqrt{\varepsilon_\alpha^2 + \Delta^2}$; $\beta = 1/T$; δ is the mean-level spacing; and Γ is a broadening parameter which accounts for scattering or recombination processes, escape rates from nanoparticles, instrumental broadening, etc. The sum over α previously is restricted to energies less than the Debye energy (E_D). ε_α denotes the energy levels of the one-body problem, which in our case are the eigenvalues of the Schrodinger equation in a close to hemispherical particle.

In order to compare the experimental tunneling conductance spectra with the theoretical formalism of SPA (see Fig. 3), we calculate dI/dV or G(V) by substituting Eqs. (3a) in Eq. (1).

2. Superconducting energy gap

Experimentally the superconducting energy gap is obtained by fitting the experimental G(V) with the theoretical expression given by Eqs. (1) and (2). This experimental gap is compared to the theoretical prediction within the SPA approach. We note first that since our model includes TFs the gap is described by a certain distribution function. The moments of this distribution are related to the spectral gap measured in the experiments. When fluctuations become important there is a certain ambiguity in the definition of the gap as different definitions lead to the same gap in the bulk limit. However these differences should be small. Keeping this in mind, we have chosen the correlation function

$$\Delta^2_{\mathrm{SPA}} = (\delta\lambda)^2\sum_{\alpha,\alpha'>0}\langle c^\dagger_\alpha c^\dagger_{\alpha'} c_{-\alpha'} c_{-\alpha}\rangle - [\langle c^\dagger_\alpha c_\alpha\rangle\langle c^\dagger_{-\alpha} c_{-\alpha}\rangle - \langle c^\dagger_{-\alpha} c_{\alpha'}\rangle\langle c^\dagger_\alpha c_{-\alpha'}\rangle].$$

Using the explicit expression for the SPA partition function [Eq. (3b)], it is possible to rewrite the previous expression as

$$\Delta^2_{\mathrm{SPA}} = \left(\frac{z}{z_0}\right)^{-1}\int d\Delta\, e^{-\beta A(|\Delta|)}|\Delta|^3 \times\left[\lambda\sum_\alpha\frac{\tanh(\beta\xi_\alpha/2)}{2\xi_\alpha}\right]^2. \quad (4)$$

Since thermal phonons are less effective to pair electrons, the electron-phonon interaction strength (λ) decreases as temperature increases. In order to simulate this effect the value of λ we use for each temperature is the result of a simple quadratic interpolation between the values of λ at low temperature and those around the critical temperature. The values of λ used in the interpolation were obtained by fitting

the experimental dI/dV with the theoretical G(V) [Eqs. (1) and (3a)] obtained by the SPA approximation.

We will use the theoretical expression 4 to obtain energy gaps from the SPA approach, which are compared with the experimental energy gap (see Fig. 4).

B. $T \ll T_c$: Deviations from mean-field predictions and the Richardson formalism

At low temperatures ($T \ll T_c$), QFs of the order parameter and other types of finite-size corrections not included in SPA (in this limit SPA is equivalent to mean field) can become important. Therefore, to calculate the low temperature behavior of the superconducting nanoparticles we proceed in the following way. We start with the BCS gap equation for a hemispherical particle of height h which can be recovered by a zeroth-order saddle point calculation of the partition function [Eq. (3b)]. This leads to

$$\partial_{|\Delta|} A(\Delta) = 0 \Rightarrow \lambda^{-1} = \sum_{\alpha} \frac{\tanh(\beta\xi_\alpha/2)}{2\xi_\alpha}, \tag{5}$$

where the sum is again restricted to the interval $[-E_D, E_D]$ around the Fermi energy. This mean-field approach breaks down as the energy gap becomes comparable with the mean-level spacing. In our experiments this occurs for $h < 20$ nm.

In this region the Richardson formalism,[34] valid at $T = 0$, is a powerful tool to describe deviations from mean-field results. For instance it was found that for $\delta/\Delta_0 < 1$ (where Δ_0 is the solution of (5) in the bulk limit), deviations in the energy gap due to QFs are very small $\sim(\Delta/E_D)(\delta/\Delta)$ (E_D is the Debye energy).[35,36] The energy gap is therefore strongly modified by QFs only for $\delta/\Delta > 1$. We can safely neglect the role of QFs on Δ since $\delta/\Delta > 1$ corresponds to heights <5 nm close to the minimum size experimentally studied here. The second important result from the Richardson's formalism is that the leading finite-size correction (δ/Δ_0) to the mean-field limit is a blocking effect that can be implemented by simply removing the two levels closest to Fermi level from the usual BCS gap equation.[35] This implies that for grains with an odd number of particles the state occupied by the unpaired one does not participate in pairing (see Appendix (3) for details).

For nanoparticles, E_F and especially E_D depend on the particle size. However in all our calculations we stick to the values of bulk Pb since its size dependence is relatively weak and poorly understood theoretically. Hence, a theoretical modeling of the size dependence of these quantities would involve the introduction of additional free parameters that would weaken the applicability of the theory. The resulting theoretical expression of the gap is valid up to corrections of the order $\sim(\delta/\Delta_0)^2$, which for Pb nanoparticles implies a size regime $h > 5$–6 nm. In order to mimic the effect of dynamical phonons present in the Eliashberg formalism used to describe a strong coupling superconductor, we employ size-dependent electron-phonon interaction strength (λ). A simple quadratic interpolation scheme is employed using λ obtained from fitting of the experimental G(V) at $T \ll T_c$ with the SPA G(V) given by Eqs. (1) and (3a) (see Appendix (4) for details). In addition according to the experimental results, in Pb grains fluctuations of the energy gap caused by shell effects in the spectral density as a function of the particle size are small[14] in comparison with those of Sn. This is not surprising as inelastic scattering and other quantum decoherence effects that shorten the coherence length, and consequently suppress shell effects,[14,17] are enhanced in strongly coupled superconductors such as Pb. As a consequence of this, in our theoretical model we have smoothed out these fluctuations and have not taken into account other coherence effects such as the size dependence of the chemical potential and matrix elements.

Based on the preceding facts we calculate theoretically the particle size variation of Δ at low temperatures [Fig. 1(c)] by solving exactly the gap [Eq. (5)] for a close to hemispherical grain (this accounts for BCS mean-field finite-size effects) but including the previously mentioned blocking effect, which accounts for the leading deviations from mean field.

IV. RESULTS AND DISCUSSIONS

After the theoretical introduction and the description of the experimental methods we are now ready to compare theory and experiment. We start with the evolution of superconductivity with particle size in the low temperature limit.

A. Evolution of the energy gap with the particle size in the low temperature limit

Figure 1(c) (solid symbols) shows the particle-size variation of the superconducting energy gap (Δ) at low temperatures ($T \ll T_c$) obtained from fitting the experimental tunneling spectra with the Dynes ansatz [Eqs. (1) and (2)]. We observe that Pb particles larger than 20 nm show a superconducting gap similar to bulk Pb ($\sim$1.36 meV), which gradually decreases with reduction in particle size. As was explained in the previous section such gradual decrease of Δ with particle size can be modeled theoretically by considering finite-size corrections within a mean-field approach and the leading corrections to the mean field formalism itself. For this purpose we use the theoretical treatment discussed in Sec. III B to calculate the particle size variation of Δ.

The black solid line in Fig. 1(c) shows the theoretical prediction for the superconducting gap obtained for the electron-phonon interaction strength λ fixed to the Pb-bulk value ($\lambda = 0.385$). It nicely reproduces the decrease of Δ for diminishing sizes, which is in qualitative agreement with the experimental data. It is important to stress here that there are no input parameters included apart from the experimentally measured shape of the particles. The red line plot in Fig. 1(c) shows how the small discrepancy between experiments and theoretical predictions vanishes when including λ variation with particle size (see Appendix (4)). Therefore, our results reveal that the observed evolution of Δ with particle size in Pb nanoparticles can be mostly explained just by invoking finite-size effects.

B. TFs and a finite gap for T > T_c

For higher temperatures (1.3–8 K) superconducting properties were also investigated by acquiring dI/dV for the Pb nanoparticles of different sizes at different temperatures. Figures 2(a) and 2(c) show the tunneling spectra for two particles 23 and 10.5 nm high. Each spectrum is first fitted using the Dynes ansatz [Eqs. (1) and (2)] giving the experimental Δ(T) and $\Gamma(T)$ as a function of temperature for each particle

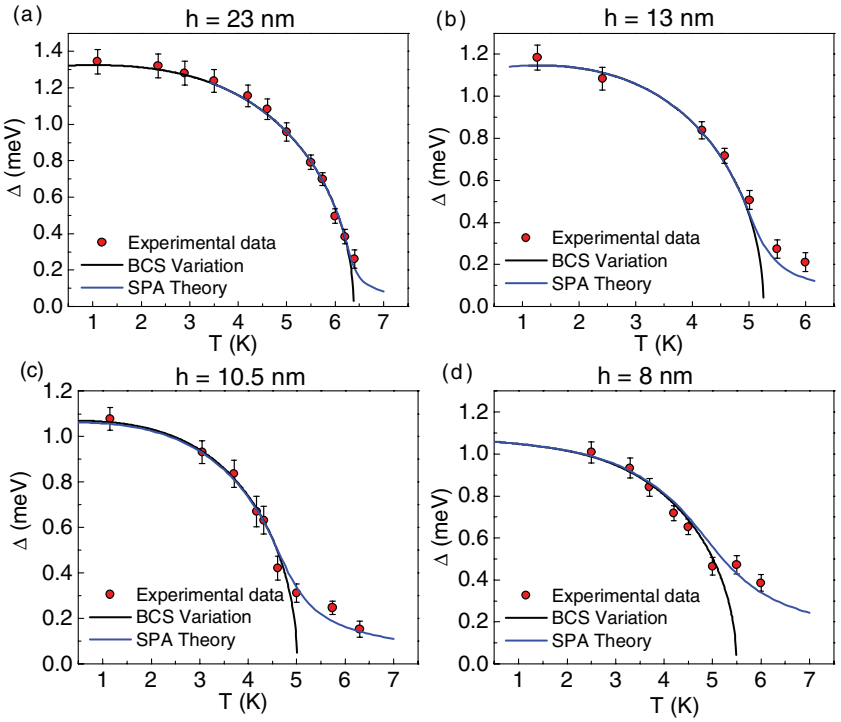

FIG. 4. (Color online) Superconducting gap $\Delta(T)$ vs temperature (T) for different nanoparticles. Red circles show the experimental gap obtained from Eq. (1) with the DOS given by Eq. (2). Solid black lines correspond to the variation expected from BCS theory. Solid blue lines show the theoretical prediction, which includes the effect of TFs within the static path approach [see Eq. (4)]. (a) $h = 23$ nm, (b) $h = 13$ nm, (c) $h = 10.5$ nm, and (d) $h = 8$ nm.

[Figs. 2(b) and 2(d)]. From Figs. 2(b) and 2(d) we observe that the evolution of Δ(T) is quite different for the two particles. While for the large particle it follows the characteristic BCS variation (black solid line), for the small particle clear deviations from BCS are visible at high temperatures. We also observe a finite energy gap beyond the mean field T_c (where T_c is defined as the temperature where the mean-field BCS gap goes to zero). As was already discussed in the introduction, we expect TFs, controlled by the parameter δ/T_c, to induce deviations from mean-field predictions. Therefore the critical region [$\propto (\delta/T_c)^{1/2}$] around T_c becomes experimentally accessible for sufficiently small ($h \leqslant 13$ nm) Pb nanoparticles.

We note TFs around T_c are well described within SPA where only paths that are space and time independent are included in the partition function. The resulting theoretical expression for the energy gap from the SPA formalism is given by Eq. (4). Figures 3(a) and 3(b) show the experimental tunneling spectra for $h = 10.5$ nm and $h = 8$ nm, respectively, at different temperatures fitted with the theoretical expression given by SPA. SPA theory nicely reproduces the experimental data. Since TFs are explicitly included in the SPA formalism, this implies that we identify the evolution of the tunneling DOS in small superconducting particles due to the influence of TFs.

We would like to point out here that for the small Pb nanoparticles at temperatures close to and above T_c, the conductance varies by a very small amount (1–8%). Nevertheless, as shown in the insets of Figs. 2(a) and 2(c) and 3(a) and 3(b) the quality of the fits close to and above T_c is still very good, allowing us to extract unique values of the experimental superconducting energy gaps for this crucial temperature window.

In Figs. 4(a)–4(d) we show the temperature evolution of the gap for four particle sizes ($h = 23$ nm, 13 nm, 10.5 nm, and 8 nm). Here the symbols are obtained from the Dynes fits to the experimental tunneling spectra. The blue solid line is the theoretical expression using the SPA formalism [Eq. (4)]. Again, we observe that while for the larger particles ($h \gtrsim 14$ nm) the energy gap follows the expected BCS functional form (black solid line) for almost all temperatures; for the smaller ones the $\Delta(T)$ has a significant tail for T $> T_c$. Thus, we can conclude from our results that TFs lead to a "fluctuation dominated regime" characterized by a finite energy gap beyond T_c that persists up to a temperature $T^*(>T_c)$. Theoretically the energy gap should be finite even for higher temperatures. However its experimental detection is challenging as it becomes difficult to separate the signal from the background noise.

V. RELIABILITY OF DYNES FITTING AND ANALYSIS OF THE BROADENING PARAMETER $\Gamma(T)$ IN THE CASE OF NANOPARTICLES

In this last section we show the validity of the data analysis by Dynes expression in the nanoscale regime. We note that the agreement between theory and experiments found in the previous section is an indication that this is the case. This check is also important in order to support our claim that deviations from mean-field predictions in the superconducting energy gap [Figs. 2(b) and 2(d)] are caused by TFs. We proceed by fitting the DOS in the SPA approach [Eq. (3a)] (which accounts for TFs) for different particle sizes with Dynes expression [see Fig. 5(a)]. The good agreement between the energy gaps obtained from Dynes fits and SPA theoretical prediction [Eq. (4)] indicates that the Dynes ansatz [Eq. (2)] is suitable in the nanoscale region and captures the effect of TFs. This also justifies our data analysis using the Dynes ansatz in this region. In addition such a good agreement also clearly confirms that the deviations from mean-field results observed in experiments [Figs. 2(b) and 2(d) fitted using Dynes ansatz] are caused by TFs.

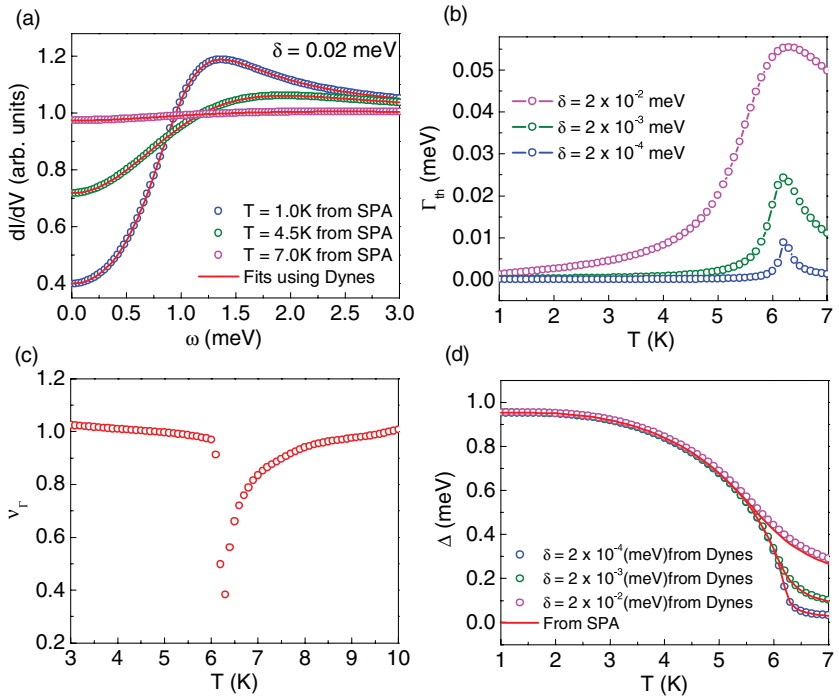

FIG. 5. (Color online) (a) Fit of the Dynes expression (red curves) to the dI/dV SPA prediction (open circles) for $\lambda = 0.34$, $\delta = 0.02$ meV, and for different values of the temperature, (b) $\Gamma_{\rm th}$, which quantifies TFs as a function of temperature for different values of δ. TFs clearly increase as δ increases (i.e., as particle size decreases). The typical width of the peak provides an estimation of the region for which deviations from mean-field results are more important. (c) The exponent ν_Γ for small δ describes the dependence of $\Gamma_{\rm th}$ on δ through the expression $\Gamma_{\rm th} \sim \delta^{\nu_\Gamma}$. The change observed around T_c indicates a qualitative enhancement of the TFs in this region. (d) Comparison between the SPA prediction (red curves) for the superconducting energy gap and those obtained by using Dynes expression to fit the dI/dV obtained by the SPA approach (open circles) for different particle sizes (different δ).

It is worth noting that in the Dynes expression the phenomenological parameter $\Gamma(T)$, which is the energy scale related to the phonon recombination and scattering and escape rates, also has contributions from TFs that peaks at T_c. However, in the range of sizes we are investigating, a quantitative analysis of TFs by the experimental variation of $\Gamma(T)$ is much more difficult to carry out than the one presented here for $\Delta(T)$.

Nevertheless, we can still show that in the case of nanoparticles $\Gamma(T)$ also contains information about the presence of TFs. To this end, it is helpful to write Γ_D, the value of Γ obtained by Dynes fitting $\Gamma(T) \equiv \Gamma_D = 1/\tau + \Gamma_{\rm th}$, where τ is the finite lifetime of the quasiparticles and $\Gamma_{\rm th}$ is the energy scale associated with TFs. We note that $\Gamma_{\rm th}$ is a finite-size effect and not related to τ. It is expected that the maximum contribution to $\Gamma_{\rm th}$ due to TFs should occur at T_c where, according to the mean-field prediction, the energy gap vanishes.

In bulk strongly coupled superconductors such as Pb, the mean-field Eliashberg's formalism provides a useful tool to compute τ due to scattering or recombination processes (see Eqs. 11, 12, 18, and Fig. 7 of Ref. 33). For Pb, good agreement between theory and experiment was found.[32,37] The total broadening in Pb increases with T. Around T_c it is approximately $1/\tau \approx 0.1$ meV.

In nanograins the possibility of escape from the particle provides an additional mechanism that reduces the lifetime. In addition a small instrumental broadening also contributes to Γ_D. The substrate is an insulator, but electrons can escape from the nanoparticles to the underlying metallic Rh substrate by either quantum tunneling or thermal activation. The former depends on the ratio of surface-to-volume and therefore will increase as the grain size is reduced. The latter will obviously increase with temperature. Although an accurate computation is not possible we expect that, in the range of sizes investigated here, the combined effect of all mechanisms contributing to quasiparticle lifetime (and thus to Γ_D through $1/\tau$) will be $\gtrsim$0.2 meV for $h < 20$ nm. In order to make an estimation of the contribution of TFs ($\Gamma_{\rm th}$) to the total energy broadening Γ_D we fit the theoretical SPA prediction of dI/dV by Dynes expression. Figure 5(a) presents points generated by the SPA formula with a constant density of single particle states for fixed $\lambda = 0.34$ and $\tau^{-1} = 0.4$ meV and their fits by the Dynes expression for different values of T. The excellent agreement obtained for all temperatures is a clear indication that Dynes expression can still be used in the nanoscale regime. Figure 5(b) shows the temperature dependence of $\Gamma_{\rm th}$, extracted from the fits as $\Gamma_{\rm th} = \Gamma_D - \tau^{-1}$, for different values of δ. We observe a peak around the critical temperature, which becomes broader as δ increases, corroborating that $\Gamma_{\rm th}$ is associated with TFs.

The scaling of $\Gamma_{\rm th}$ with the mean-level spacing δ and hence particle size [see Fig. 5(c)] strongly depends on the temperature. $\Gamma_{\rm th} \propto \delta$ for $T \ll T_c$. It is possible to show that this behavior agrees with the analytical prediction obtained considering higher order corrections to the mean-field solution within the SPA approximation. As was expected, near the mean field T_c TFs becomes more important. It is possible to identify a region of size proportional to $T_c\,(\delta/T_c)^{\nu_\Gamma}$, $\nu_\Gamma < 1$, around T_c where deviations from mean-field results are not negligible.

In Fig. 5(d) the values of the fitted Dynes energy gap (Δ) are compared with the theoretical prediction for the energy gap in the SPA approach [Eq. (4)]. The agreement is excellent. Moreover they were found to present the same finite-size scaling behavior. These results are a further confirmation that the analysis of the experimental data by Dynes expression captures correctly the physics of TF. The lifetime of quasiparticles due to decoherence processes and interactions $1/\tau = 0.4$ meV was taken to be constant in this simple example. For a realistic

model it should increase with T in a monotonic way, i.e., it should not be sensitive to the phase transition.

VI. CONCLUSIONS

To summarize we report direct evidence of TFs and the gradual breakdown of superconductivity in Pb nanoparticles as the size is reduced. The experimental data is well described by a theoretical model that includes TFs, mean-field finite-size effects, and leading corrections to the mean-field formalism. TFs give rise to a finite-energy gap or "fluctuation dominated regime" around T_c. Our results are a first step to understand quantitatively the evolution of superconductivity with particle size and the role of TFs for single small superconductors.

APPENDIX

1. Growth and shape of the nanoparticles

The main goal of the present work is to address the superconducting properties of single isolated Pb nanoparticles. This requires the growth of nanoparticles on a substrate with no electronic states close to the Fermi level and to have these particles well separated from each other. Thus, the BN/Rh(111) system presenting an ultrathin insulating BN layer with a band gap of ~6 eV represents an ideal surface for the growth of the particles and for carrying out STM/STS experiments. To prepare the BN/Rh(111), we obtained a clean Rh(111) surface by repeated annealing and argon-ion sputtering cycles. The clean surface was then exposed to a 40 l (1 l = 10^{-6} Torr s) dose of Borazine gas with the substrate temperature held at 1070 K. This procedure leads to the formation of a BN-insulating layer on top of the metallic substrate with complete monolayer coverage.[30]

Once the BN/Rh(111) surface was formed, nanometer-sized Pb particles were deposited on top of it by using BLAG, which is known to produce small particles with narrow size distribution. We first adsorbed a Xe-buffer layer on the BN/Rh(111) surface at 50 K, then evaporated Pb on top of the Xe, and finally desorbed the Xe layer by warming up the sample to room temperature. Pb nanoparticles form directly on the Xe-buffer layer due to the reduced interaction with the substrate and grow in size during Xe desorption due to cluster coalescence until making contact with the surface. The final size of the nanoparticles can be tuned by adjusting the amount of deposited Pb and the buffer-layer thickness. In order to study a wide range of nanoparticle sizes, we used two different sets of preparation parameters: 0.5 ML of Pb with 3000 l Xe and 2.0 ML of Pb with 15 000 l of Xe. This produced isolated Pb nanoparticles with heights between 3 and 30 nm.

The shape of these Pb nanoparticles has been considered to be approximately hemispherical. In order to verify this we developed a very simple model, shown in Fig. 6 (inset). The model assumes a hemispherical nanoparticle of radius r and a spherical tip apex of radius R. z and z_0 represent the tip-particle and tip-substrate tunneling distances, respectively. According to this model, the ratio between apparent nanoparticle height (H) and the convoluted full width (D) is

$$H/D = (r + z - z_0)/2\sqrt{(R + r + z)^2 - (R + z_0)^2} \tag{A1}$$

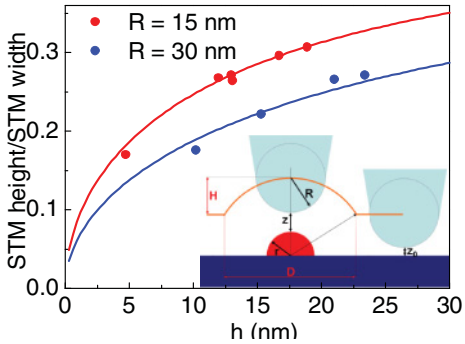

FIG. 6. (Color online) Plot of the experimental STM height/STM width as a function of the nanoparticle height h for two different tips (red and blue). Solid circles denote the experimental data. Solid lines are the fits obtained using Eq. (A2). The inset shows a schematic of the model used (see text).

If we assume that the tip and particle radii are much larger than the tunnelling distances z and z_0 (~1 nm), then $H = r + z - z_0 \cong r$ and (A1) can be simplified to

$$\frac{H}{D} \cong \frac{r}{2}\sqrt{r\,(r + 2R)} \tag{A2}$$

This expression with only one free parameter (R) can be used to directly compare with experiments, as the observed STM height H is very closely related to the particle radius r. To prove the hemispherical shape of the nanoparticles we have fitted the ratio H/D (STM height/STM width) as a function of the nanoparticle height H as obtained experimentally from the STM topographic images. This comparison must be restricted to nanoparticles of sizes similar to tip apex radii ($R \sim r$), otherwise the tip convolution would hide any real feature of the nanoparticles. In Fig. 6 the ratio H/D is plotted for two different sets of nanoparticles corresponding to two large-scale STM images (blue and red) in which the tip did not change during the scan. This ensures that all the nanoparticles in the particular topographic image are measured with the same tip radius R ($R = 30$ nm for blue and $R = 15$ nm for red). Both sets of nanoparticles can be nicely fitted by means of the previous expression (A2), confirming that the shape of the Pb nanoparticles is close to a hemisphere.

2. Experimental resolution and fitting procedure of the experimental conductance spectra by Dynes ansatz

The experimental output $G(V)$, i.e., dI/dV spectrum, was fitted by a standard algorithm that minimizes the square of the difference between the experimental data and the $G(V)$ given by the Dynes ansatz [Eqs. (1) and (2)]. All points considered in the fitting carry the same weight. We obtain the experimental values for the energy gap Δ and the quasiparticle energy broadening Γ_D from the fitting. As can be observed in Fig. 2, Dynes fitting provides an excellent description of the experimental data. However an important point of the fitting procedure is described subsequently.

The raw experimental data is rescaled so that $G(V)$ goes to unity for large voltage bias (V). For small particles $h < 10$–14 nm and high temperature ($T \geqslant T_c$) we have observed that Γ_D, the value of Γ obtained by Dynes fitting, is quite sensitive to small changes in the rescaling of $G(V)$ and the

fitting interval. This is not surprising as the dip in $G(\mathrm{V})$ at $\mathrm{V} \sim 0$ is quite weak with respect to the background noise. Therefore small errors in the rescaling have a strong impact in the value of the fitting parameters, especially Γ_D. In order to overcome this problem we have added a third fitting parameter that sets the rescaling of $G(\mathrm{V})$. It is also necessary to carry out the fitting in a bias voltage interval that does not go much beyond the value of Δ. We found that in most cases a 3-meV interval (from the origin) is a sensible compromise.

Broadening Γ of the dI/dV spectra measured on the Pb superconducting nanoparticles is mainly due to intrinsic sources (scattering or recombination processes, thermal and QFs, escape rates from nanoparticles) with minor contributions from extrinsic sources (the ac voltage modulation and instrumental noise). In order to calibrate the contribution to the broadening Γ from the extrinsic sources and thus obtain an upper limit to the contribution to Γ due to our instrumental noise, we have acquired dI/dV spectra with exactly the same tunneling parameters as for Pb nanoparticles on a bulk-Pb sample. Open squares in Fig. 1(b) correspond to a dI/dV spectra measured on bulk Pb at 1.5 K, which has been fitted using the same broadened BCS DOS as the one used for the Pb nanoparticles [Dynes ansatz, Eqs. (1) and (2)]. The best fit to the experimental data, which includes the 50-μV ac voltage modulation and the Fermi-Dirac broadening, gives a superconducting gap $\Delta = 1.36$ meV, matching perfectly with the expected one for bulk Pb, and a broadening parameter $\Gamma = 10$–20 μV. Therefore, we can estimate the maximum contribution due to our experimental noise to the broadening Γ of our dI/dV spectra to be 20 μV. This value is one order of magnitude lower than the smallest Γ that we have obtained on the Pb nanoparticles, which ensures that Γ is mostly related to intrinsic sources in these nanoparticles. Moreover, our experimental system is very carefully shielded with respect to high-frequency (RF) voltage noise, which makes our effective temperature coincide (within 20 mK) with the actual temperature of the STM. The measurement of the superconducting critical temperature for bulk Pb was ultimately used to verify the calibration of the sample temperature. By measuring the evolution of Δ with temperature on a Pb-bulk sample an expected T_c value of 7.25 K was obtained.

We would like to point out that for the small Pb nanoparticles at temperatures close to and above T_c, the conductance varies by a very small amount (1–8%). Inspite of this, the quality of the fits to the spectra measured for the Pb nanoparticles with the Dynes expression close to and above T_c is very good. For each spectrum we use the least-square fitting routine to minimize the χ^2 to obtain Δ and Γ for the best fit. We also take particular care to determine the uniqueness of the fits. As a representative, we show below the fitting done for the spectra measured on the 10.5-nm particle of Fig. 2(c) at $T = 5.74$ K. It is worth noting that in this spectrum the conductance varies by only 2%, since it is measured well above T_c ($T_c = 5.0$ K for such a particle). Minimizing χ^2 we obtain the best fit for $\Delta = 0.21$ meV and $\Gamma = 0.38$ meV. To test the uniqueness of the fit, we change Γ (within a range) to compensate for the change in Δ. It can be seen that the curve is reasonably fitted only with values of Δ and Γ in a particular window of values (see Fig. 7). This gives us the error bars in Δ and Γ, which are shown in Figs. 2(b) and 2(d).

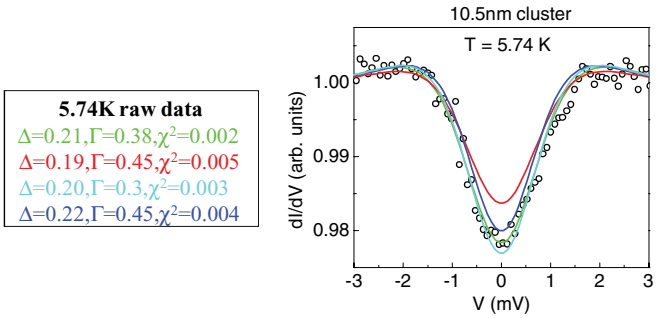

FIG. 7. (Color online) Normalized dI/dV spectrum measured on Pb nanoparticle of height 10.5 nm at 5.74 K (black open circles). The fits to the data (solid lines) have been done using the Dynes expression (see main text) where the different lines are obtained with different fitting parameters. Best fit was obtained for $\Delta = 0.21$ meV and $\Gamma = 0.38$ mV with a $\chi^2 = 0.002$ (green line).

3. Finite-size effects included in the theoretical formalism (for $T \ll T_c$)

Two distinct types of finite size effects in the one particle DOS were considered in the comparison with experimental results.

A. Spectral fluctuations

The first type of finite-size corrections are simply mean effects related to the fact that, in superconducting nanoparticles, the spectral density of the one body problem is not constant in the interacting region around the Fermi level. A complete analytical treatment of these corrections, valid for any particle shape, was recently developed.[17] In practical terms these deviations are taken into account by considering explicitly the spectrum of the one body problem. In our case the particle can be modeled as a spherical cap of height h and radius R with $R \sim h$. We compute the spectrum numerically for a given ratio of h/R. In the hemispherical case $h/R = 1$, the eigenvalues are simply the roots of a Bessel function. For other ratios we use a method based on a perturbative expansion[38] around the hemispherical geometry, which is valid for $1 - h/R \ll 1$.

B. Blocking effects

As the particle size is reduced to the point that δ becomes comparable to the bulk gap, finite-size effects induce deviations from mean-field predictions. In the limit of vanishing temperatures the solution of the Richardson's equations[34,39] provide an exact account of the ground state and low energy excitations of the usual BCS Hamiltonian. Recently it was shown,[35] from the exact Richardson's equations, that the leading correction (δ/Δ) to mean field has a simple interpretation within the mean-field formalism: it is equivalent to removing two levels closest to the Fermi energy in the usual BCS gap equation (for a previous derivation of this result by using path integral methods see Ref. 36). Physically this is expected as the gap can be defined as the minimum energy to break a pair. In a finite system, as a result of the pair breaking, two electrons will occupy levels around the Fermi energy giving rise to a blocking effect in the sense that no pairing is possible at these energies. Using this we include the leading correction to mean field by simply removing the two levels closest to the Fermi energy in

the definition of the action of our system. It was also shown in Ref. 35 that for $\delta/\Delta < 1$, QFs, not included in our formalism, are at most of order $\sim(\Delta/E_D)(\delta/\Delta)$, which extends the applicability of our model until particle sizes $h \sim 6$ nm very close to the smallest particles, which can be studied experimentally.

4. Size dependence of the electron-phonon interaction parameter (λ)

In our model λ is an effective parameter that describes the strength of the interactions that lead to the superconducting state. It is well documented that in strongly coupled superconductors, such as Pb, λ decreases with temperature as thermal phonons are less effective to glue electrons together. The dependence of λ on grain size is less clear, as in the nanoscale region several competing effects must be considered. Coulomb interactions and quantization effects in the phonon spectrum increase as the grain size is reduced. As a result we expect the effective coupling constant to decrease accordingly. On the other hand the increasing contribution of surface phonons as system size is reduced is expected to increase λ.

In order to make quantitative comparisons between theory and experiment it is thus necessary to employ a size-dependent coupling constant. It is possible to estimate this size dependence by fitting the experimental differential conductance with the theoretical prediction from SPA approach where λ is a fitting parameter. In Fig. 1(c) we show the results of the fitting in the low temperature limit $T = 1$–1.25 K. We observe that for the largest grains the value of the coupling constant leads to an energy gap very close to the bulk one ∼1.35 meV. As a general rule the coupling constant decreases with the system size (Fig. 8). However the size dependence for $h > 6$–7 nm is relatively weak, $\leqslant 5\%$. It is tempting to speculate that the flattening observed for $h \sim 10$ nm is due to the interplay between surface-phonons effects that enhance pairing and the rest of effects that tend to weaken it. We note [see Fig. 1(c)] that quantitative agreement between theory and experiment is only achieved after this small size dependence of λ is included in the theoretical model.

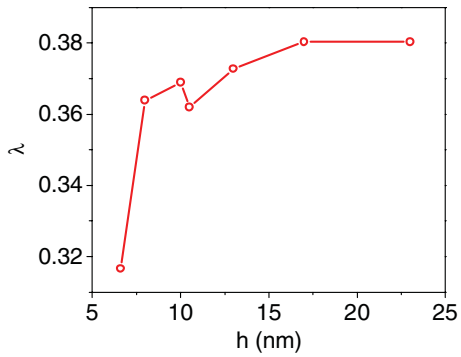

FIG. 8. (Color online) λ as a function of the particle size (h). This result was obtained by fitting the experimental differential conductance by theoretical prediction of the SPA approach where λ is a fitting parameter. The particle is close to hemispherical $h \sim R$.

*amg73@cam.ac.uk
†Present address: Max Planck Institute for the Physics of Complex Systems, Dresden, D-01187, Germany.
‡sangita.bose@gmail.com

[1] B. Abeles, R. W. Cohen, and G. W. Cullen, Phys. Rev. Lett. **17**, 632 (1966).
[2] M. Strongin, O. F. Kammerer, J. E. Crow, R. D. Parks, D. H. Douglass, and M. A. Jensen, Phys. Rev. Lett. **21**, 1320 (1968).
[3] I. Giaever and H. R. Zeller, Phys. Rev. Lett. **20**, 1504 (1968).
[4] D. C. Ralph, C. T. Black, and M. Tinkham, Phys. Rev. Lett. **74**, 3241(1995).
[5] A. Bezryadin, C. N. Lau, and M. Tinkham, Nature **404**, 971 (2000).
[6] A. A. Shanenko, M. D. Croitoru, and F. M. Peeters, Europhys. Lett. **76**, 498 (2006).
[7] T. Nishio, M. Ono, T. Eguchi, H. Sakata, and Y. Hasegawa, App. Phys. Lett. **88**, 113115 (2006).
[8] T. Nishio, T. An, A. Nomura, K. Miyachi, T. Eguchi, H. Sakata, S. Lin, N. Hayashi, N. Nakai, M. Machida, and Y. Hasegawa, Phys. Rev. Lett. **101**, 167001 (2008).
[9] I. Guillamon, H. Suderow, A. Fernández-Pacheco, J. Sesé, R. Córdoba, J. M. De Teresa, M. R. Ibarra, and S. Vieira, Nature Phys. **5**, 651 (2009).
[10] C. Brun, I-Po Hong, François Patthey, I. Yu. Sklyadneva, R. Heid, P. M. Echenique, K. P. Bohnen, E. V. Chulkov, and Wolf-Dieter Schneider, Phys. Rev. Lett. **102**, 207002 (2009).
[11] T. Cren, D. Fokin, F. Debontridder, V. Dubost, and D. Roditchev, Phys. Rev. Lett. **102**, 127005 (2009).
[12] K. Wang, X. Zhang, M. M. T. Loy, T.-C. Chiang, and X. Xiao, Phys. Rev. Lett. **102**, 076801 (2009).
[13] T. Zhang, P. Cheng, W.-J. Li, Y.-J. Sun, G. Wang, X.-G. Zhu, K. He, L. Wang, X. Ma, X. Chen, Y. Wang, Y. Liu, H.-Q. Lin, J.-F. Jia, and Q.-K. Xue, Nature Phys. **6**, 104 (2010).
[14] S. Bose, A. M. García-García, M. M. Ugeda, J. D. Urbina, C. H. Michaelis, I. Brihuega, and K. Kern, Nature Mat. **9**, 550 (2010).
[15] J. von Delft, Ann. Phys. **10**, 219 (2001).
[16] V. Z. Kresin and Y. N. Ovchinnikov, Phys Rev. B **74**, 024514 (2006).
[17] A. M. García-García, J. D. Urbina, E. A. Yuzbashyan, K. Richter, and B. L. Altshuler, Phys. Rev. Lett. **100**, 187001 (2008).
[18] D. Innocenti, N. Poccia, A. Ricci, A. Valletta, S. Caprara, A. Perali, and A. Bianconi, Phys. Rev. B **82**, 184528 (2010).
[19] P. W. Anderson, J. Phys. Chem. Solids **11**, 26 (1959).
[20] W.-H. Li, C. C. Yang, F. C. Tsao, and K. C. Lee, Phys. Rev. B **68**, 184507 (2003).
[21] S. Reich, G. Leitus, R. Popovitz-Biro, and M. Schechter, Phys. Rev. Lett. **91**, 147001 (2003).
[22] S. Bose, P. Raychaudhuri, R. Banerjee, P. Vasa, and P. Ayyub, Phys. Rev. Lett. **95**, 147003 (2005).
[23] S. Bose, C. Galande, S. P. Chockalingam, R. Banerjee, P. Raychaudhuri, and P. Ayyub, J. Phys. Condens. Matter **21**, 205702 (2009).
[24] T. Tsuboi and T. Suzuki, J. Phys. Soc. Jpn. **42**, 437 (1977).
[25] R. A. Buhrman and W. P. Halperin, Phys. Rev. Lett. **30**, 692 (1973).
[26] E. Bernardi, A. Lascialfari, A. Rigamonti, L. Romanò, V. Iannotti, G. Ausanio, and C. Luponio, Phys. Rev. B **74**, 134509 (2006).
[27] W. J. Skocpol and M. Tinkham, Rep. Prog. Phys. **38**, 1049 (1975).
[28] B. Mühlschlegel, D. J. Scalapino, and R. Denton, Phys. Rev. B **6**, 1767 (1972).

[29]R. Denton, B. Mühlschlegel, and D. J. Scalapino, Phys. Rev. B **7**, 3589 (1973).
[30]I. Brihuega, C. H. Michaelis, J. Zhang, S. Bose, V. Sessi, J. Honolka, M. Alexander Schneider, A. Enders, and K. Kern, Surf. Sci. **602**, L95 (2008).
[31]M. Tinkham, *Introduction of Superconductivity*, 2nd edn. (McGraw-Hill, New York, 1996), p. 75.
[32]R. C. Dynes, V. Narayanamurti, and J. P. Garno, Phys. Rev. Lett. **41**, 1509 (1978).
[33]S. B. Kaplan, C. C. Chi, D. N. Langenberg, J. J. Chang, S. Jafarey, and D. J. Scalapino, Phys. Rev. B **14**, 4854 (1976).
[34]R. W. Richardson, J. Math. Phys. **18**, 1802 (1977).
[35]E. A. Yuzbashyan, A. A. Baytin, and B. L. Altshuler, Phys. Rev. B **71**, 094505 (2005).
[36]K. A. Matveev and A. I. Larkin, Phys. Rev. Lett. **78**, 3749 (1997).
[37]P. Hu, R. C. Dynes, V. Narayanamurti, H. Smith, and W. F. Brinkman, Phys. Rev. Lett. **38**, 361 (1977).
[38]A. H. Rodriguez, C. Trallero-Giner, S. E. Ulloa, and J. Marin-Antuna, Phys. Rev. B **63**, 125319 (2001).
[39]G. Sierra, J. Dukelsky, G. G. Dussel, Jan von Delft, and F. Braun, Phys. Rev. B **61**, 11890 (2000).
[40]I. Horcas, R. Fernández, J. M. Gómez-Rodríguez, J. Colchero, J. Gómez-Herrero, and A. M. Baro, Rev. Sci. Inst. **78**, 013705 (2007).